Local mechanical and optical properties of normal and transparent root dentin

M. BALOOCH[1], S. G. DEMOS[1], J. H. KINNEY[2], G. W. MARSHALL[2*], G. BALOOCH[2], S. J. MARSHALL[2]
[1]*Lawrence Livermore National Laboratory, Livermore, CA, USA*
[2]*Division of Biomaterials and Bioengineering, Department of Restorative Dentistry, University of California at San Francisco, San Francisco, CA, USA*
E-mail: graymar@itsa.ucsf.edu

The mechanical and optical properties of healthy and transparent root dentin are compared using atomic force microscopy (AFM), micro-Raman and emission spectroscopies and fluorescence microscopy. The elastic modulus and hardness of intertubular and peritubular transparent and healthy dentin did not differ appreciably. The tubule filling material in the transparent zone, however, exhibited values between peritubular and intertubular dentin. Raman spectroscopy revealed a shift in the 1066 cm^{-1} band to 1072 cm^{-1} from normal to transparent intertubular dentin. The material filling the tubule lumen in transparent dentin showed an increase in frequency of the band near 1070 cm^{-1} as well. The emission spectral characteristics under 351 nm photoexcitation indicate differences between normal and transparent intertubular dentin. A transition region of about 300 μm between normal and transparent dentin was identified. In this region the intertubular emission properties were the same as for normal dentin, but tubules were filled. The filling material had emission characteristics closer to the normal intertubular than to transparent intertubular dentin.

1. Introduction

Non-carious lesions that occur in the form of notches in the dentin just below the enamel-cementum junction are relatively common. In addition to the loss of tooth structure, such lesions are often designated as sclerotic, transparent or irritation dentin, since mineral deposits commonly occlude the dentinal tubule lumen and presumably lead to increases in hardness, and induce changes in optical characteristics of the dentin leading to a transparent appearance. The etiology of these non-carious cervical lesions has recently been reviewed and shown to be uncertain and complex with most suggesting that the causes may be multifactorial, involving erosion, abrasion, and stress (abfraction), and increase with age [1].

Weber [2] used microradiography to study dentin sclerosis and found that translucency resulted well before all the tubules were filled with mineral. Brännström and Garberoglio [3] found many tubules completely occluded with material similar to that seen in peritubular dentin, while other tubules had varying degrees of tubule lumen reduction. Vasiliadis *et al*. [4] reported that sclerosis occurred by occlusion of dentinal tubules by mineral with a refractive index similar to that of dentin, and that translucence occurred before the majority of tubules were completely occluded. Yoshiyama *et al*. [5] found that for insensitive (sclerotic) dentin about 75% of the tubules were closed. Yagi and Suga [6] associated sclerotic changes beneath cervical lesions with the deposition of cuboidal or rhomboid-shaped, short rod- and droplet-like crystals within the tubules. Interestingly, the crystal morphology appeared to be the same for a given tubule, but differed from tubule to tubule. This suggests that the tubules in such lesions may become occluded by a continuous growth of peritubular dentin.

Furthermore, sclerotic lesions appear to respond to etching and bonding treatments differently than normal dentin, thus leading to varying responses to clinical treatment [7–9] that is probably a result of increased resistance to demineralization in sclerotic dentin due to the tubule obstruction [10]. Van Meerbeek *et al*. [11] suggested that demineralization is more difficult in both the peritubular and intertubular regions of sclerotic dentin and showed that the hybrid resin layer formed in dentin bonding is much thinner and exhibits few or no tubule tags as compared to normal occlusal dentin. Perdigao *et al*. [12] recently evaluated the shear bond strengths of adhesive systems to dentin substrates with different levels of mineralization. The shear bond strength to normal dentin was significantly higher than that of artificially hypermineralized dentin. Since these alterations are of great clinical significance and their influence on the demineralization process requires clarification, Marshall *et al*. [13] recently evaluated the

*Author to whom all correspondence should be addressed.

demineralization behavior of cervical non-carious transparent lesions, and found significant differences in the intertubular dentin response, in addition to the effect of the occluded tubules.

From the prior work it appears that apatite or other calcium phosphate mineral is deposited in the tubules of cervical non-carious or class V lesions leading to partial occlusion of the tubules. Interestingly, several investigations also suggest that changes occur in the intertubular dentin which appear to have a higher mineral content [2], and form hybrid layers that are thinner [11] and etch differently [13]. In an effort to further understand such alterations in the dentin structure, this work tested the hypothesis that the mechanical properties and chemistry of the intertubular dentin were altered in cervical transparent/sclerotic non-carious lesions. To carry out this work we used a modified form of atomic force microscopy (AFM) to independently measure the nanomechanical properties (nanohardness and elastic modulus) of the peritubular, intertubular and tubule mineral deposits in the transparent dentin for comparison with similar measurements made in normal cervical dentin. In addition, selected lesions were evaluated with micro-Raman spectroscopy that provides an insight on molecular structure and emission spectroscopies and fluorescence microscopy which provide insight into chemical composition of material.

2. Materials and methods

2.1. Sample preparation

Dentin containing non-carious cervical or transparent dentin areas and areas of normal root dentin were evaluated in this study. All teeth were extracted from research subjects requiring such extractions as part of their dental treatment. All subjects enrolled in this research have responded to an Informed Consent protocol which has been approved by the UCSF Institutional Committee on Human Research. All such extracted teeth are sterilized by gamma radiation [14] and stored in filtered and purified water at 4 °C until prepared. The teeth were used to prepare 1 to 1.5 mm thick sagittally cut dentin slices. The surface of each slice was ground through successive grits of wet polishing papers from 240 to 600 grits and polished through successive polishing pastes ending with 0.05 μm alumina powder, and ultrasonicated in water to remove remnant smear layer.

2.2. Atomic force microscopy (AFM)

A modified AFM-based indenter was used (Digital Instruments Nanoscope III, Santa Barbara, California) in which a capacitive sensor head replaces the standard AFM head including the laser, cantilever and photodetector (Triboscope, Hysitron Inc., Minneapolis, MN) as previously described [15]. The Triboscope sensor consists of two-fixed outer electrodes (drive plates) that are driven by AC signals 180 degrees out of phase relative to each other. Due to the small spacing between the two plates, the electric field changes linearly from one to the other. Therefore the electric field potential is maximum at the drive plates and zero at the center between the two plates. The center or pickup electrode is suspended in a manner that allows it to move up and down in the region between the two drive plates. The pickup electrode assumes the electric potential of the space between the two drive plates. This results in a bipolar output signal that is equal in magnitude to the input signal at the maximum deflection, and zero at the center position. The synchronous detector converts the phase and amplitude information from the sensor output into a bipolar DC output signal. The signal is therefore proportional to the pickup electrode position. In the imaging mode, the output signal is used as a feedback to the piezoceramic tube scanner for constant–force contact imaging. In the indentation mode, the feedback is turned off and a voltage ramp is applied to the lower drive plate. As a result, an electrostatic force is generated between the pickup electrode and the drive plate. The force can be expressed as,

$$F = k_e V^2 \tag{1}$$

where k_e is electrostatic force constant and V is the applied voltage. The voltage ramps are formulated to produce triangular, trapezoidal or square loading forces to the sample. In this study a trapezoidal loading force ramp was used. The force is applied to the sample through a diamond tip glued to a tapped-polymer holder attached to the pickup electrode by a small screw for experiments in air. In the imaging mode the minimum contact force applied to the sample is about 1 μN. In the indentation mode, loads up to 30 000 μN can be applied. A cube corner indenter with a tip radius of curvature of about 20 nm was used for this work.

The hardness, H, is calculated on the basis of maximum force, $F_{\max}$, divided by projected contact area at maximum load, a, and the elastic modulus, E, is calculated from the contact stiffness, S, defined as the slope of the linear portion of the force/displacement curve during unloading near the maximum load [16].

$$H = \frac{F_{\max}}{a} \tag{2}$$

$$E = \sqrt{\frac{\pi}{a}}\frac{S}{2} \tag{3}$$

2.3. Micro-Raman scattering spectroscopy

Microscopic Raman scattering measurements were performed using a microspectrometer (system 2000) from Renishaw Inc. (Cambridge, UK). Two lasers were utilized to obtain the Raman spectra having excitation wavelengths of 514.5 and 630 nm and average illumination power of 2 mW. Raman scattering profiles in 400 to 1600 cm^{-1} spectral range were obtained with overall spectra resolution of 0.5 cm^{-1}. The laser beam was focused on the sample to micron-size spot using a 100 × microscope objective lens in a confocal configuration in order to provide the necessary spatial resolution for the study of mineral associated with the tubules. Since the lumen of the tubules is filled in the transparent dentin and the diameter of the lumen is approximately 1 μm, and is surrounded by an annulus of peritubular dentin, the 1 μm spot size may have

illuminated both the material filling the lumen and portions of the peritubular dentin. The same lens was used for collection of the Raman scattered light from the sample. Using appropriate optics, light was spectrally analyzed by a single grating spectrograph and recorded using a CCD camera. The same sample and approximately the same area was used to obtain both mechanical and optical properties.

2.4. Microscopic fluorescence imaging and spectroscopy

The optical configuration of the spectroscopic system utilized to measure the emission spectra from the samples is shown in Fig. 1(a). An argon ion laser operating at 351 nm was used as the photoexcitation source. The excitation beam is coupled into a microscopic spectroscopy system using a 355 nm, 50/50 beamsplitter and is used to illuminate the sample after passing through a (25 ×) reflecting microscope objective lens. The backscattered emission light from the sample is collected by the same microscope objective lens and after passing through the beamsplitter is focused into the entrance slit of a single grating spectrograph to be spectrally analyzed. The emission spectrum is recorded using a CCD detector.

The microscopic fluorescence imaging experimental setup is shown in Fig. 1(b). The microscopic imaging system is composed of a long working distance microscope objective followed by a zoom lens and liquid nitrogen cooled CCD detector. The zoom lens provides a × 5 magnification. A set of microscope objectives were available having magnification powers of × 20 and × 10 and working distances of 20 mm and 30 mm, respectively. In this arrangement, 1 μm^2 of an object at the image plane is projected and recorded on 4 pixels of the CCD detector using the × 20 objective, while a 600 × 600 μm region of the sample was imaged. The argon laser beam was expanded to a diameter of 10 mm and the central portion of the beam was used to illuminate the sample at the section to be imaged with nearly uniform illumination intensity. An optical band-pass filter was positioned between the CCD detector and the zoom lens in order to select the desired emission band to be used for imaging, and to discriminate against the laser light scattering in the sample. Five different optical band-pass filters were used in this work: three narrow band-pass filters with central wavelength at 410 nm, 450 nm, and 490 nm having spectral bandwidth of 9 nm, and two long-wavelength-pass filters with cut-off frequencies at 450 nm and 700 nm. The spectral differences in the emission profiles from normal and transparent dentin were employed to obtain microscopic fluorescence images of the samples with near diffraction limited spatial resolution (∼ 1 μm) using the experimental set up shown in Fig 1(b).

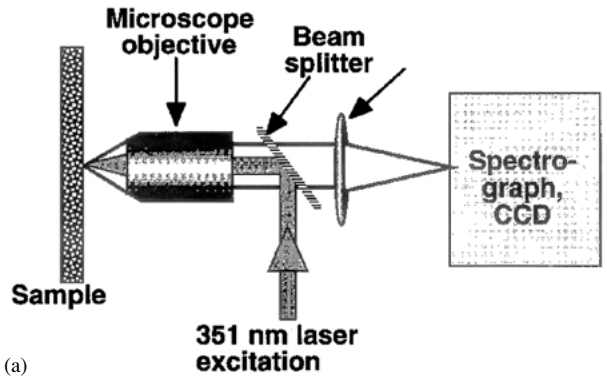

(a)

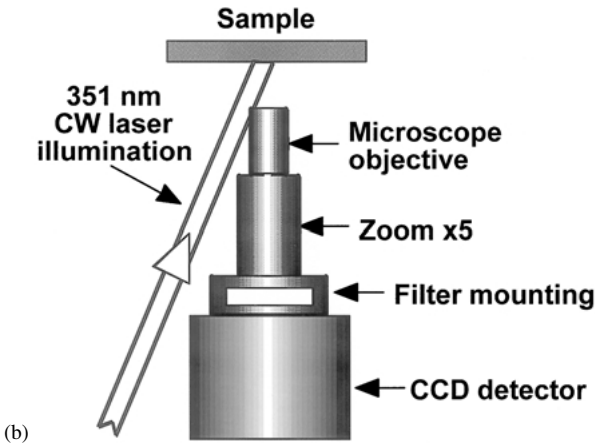

(b)

Figure 1 Schematic diagrams of experimental setups. (a) emission spectroscopy; (b) emission imaging.

3. Results

Fig. 2 shows AFM images of (a) normal and (b) transparent root dentin. In the normal dentin, tubules were mostly empty while the transparent dentin generally contained filling materials. Fig. 3 shows the indentations performed at 1 μm intervals starting from the intertubular dentin, passing through peritubular dentin and the tubule filling material. The elastic modulus, E and hardness, H are plotted with the numbers corresponding to the indentations on the AFM image. E and H values for the material filling the tubule lumen were between those of peritubular and intertubular dentin. The elastic modulus and hardness of intertubular dentin for transparent and normal dentin were the same within the experimental error. The range of E and H are given in Table I.

3.1. Micro-Raman Spectroscopy

Fig. 4 shows the Raman spectra obtained from 1 μm diameter areas of apparently normal and transparent intertubular dentin. The Raman band positions and assignments of the normal and transparent intertubular dentin for the range studied are shown in Table II.

Little difference was observed in the phosphate vibrational modes. However, transparent dentin exhibited a shift in the carbonate ion band at 1066 cm^{-1} to 1072 cm^{-1} with a decrease in intensity.

The Raman spectra of the materials associated with the tubule for normal and transparent dentin are shown in Fig. 5. In the normal dentin this is primarily from peritubular dentin, while in the transparent dentin the spectra comes primarily from the material filling the tubule lumen. Raman band positions and assignments of the normal and transparent materials for the range studied are shown in Table III.

The spectra from the transparent dentin associated with the material in the dentin tubules exhibited an

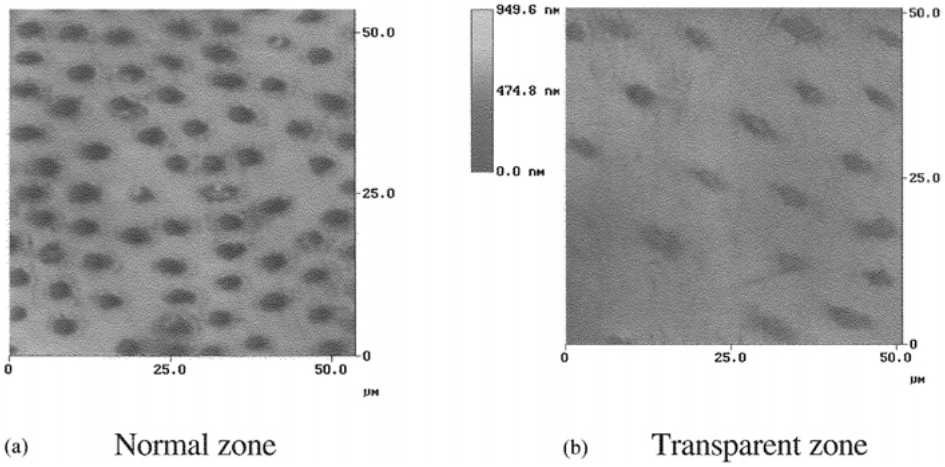

Figure 2 AFM images of normal and transparent dentin. Dentin tubules are open in normal dentin (a) and filled with mineral in the transparent dentin (b).

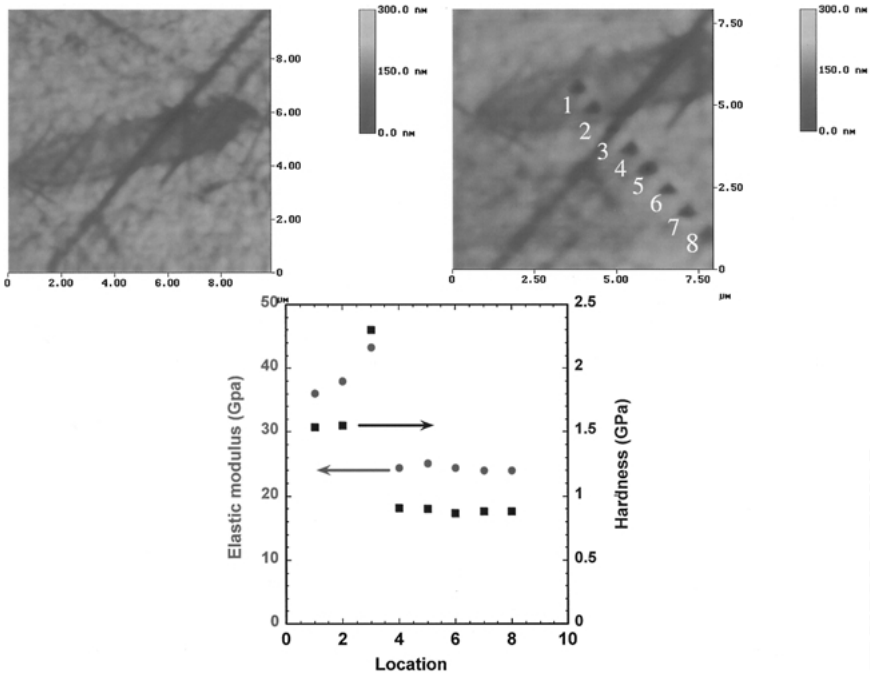

Figure 3 Nanomechanical properties of different dentin regions. AFM image (top left) showing filled dentin tubule prior to indentation, with the same area shown (top right) following indentation at 1 μm intervals from intertubular dentin through the peritubular dentin and mineral filling the tubule lumens. Resulting hardness and modulus values for each indentations are shown in the lower diagram.

increase in frequency of the carbonate ion band near 1070 cm^{-1}, compared to normal dentin, but the intensity did not change.

3.2. Emission imaging and spectroscopy

The emission spectra in the 380–730 nm spectral region arising from normal and transparent dentin near the pulp under 351 nm photoexcitation is shown in Fig. 6. The spectral profiles indicate the presence of three broad spectral features (peaks) centered at 420, 450 and 500 nm in both normal and transparent zones. However, on normal dentin, the highest intensity peak was near 500 nm, while in the transparent region, the highest intensity peak was near 450 nm. In addition, the normal region exhibited stronger emission in the red and near infra-red region as compared to the transparent region.

Fig. 7 shows the emission image of a 1.1 × 1.1 mm section of the sample covering both normal and the transparent zones obtained using the 700 nm long pass filter in front of the imaging CCD camera. Consistent with the spectral profiles shown in Fig. 6, the normal zone (left) exhibited higher intensity than the transparent zone (right) due to its enhanced emission in the near infra-red spectral region. The presence of three different regions is also seen in this image. Higher magnification of each of these regions are shown in Fig. 8, where the contrast of the images has been adjusted in order to demonstrate the differences. Fig. 8(a) shows a 100 × 180 μm section from the normal region of the

TABLE I AFM indentation results for dry dentin

Dentin area	*E* (GPa)	*H* (GPa)
Intertubular	24–25	0.5–0.8
Peritubular	40–45	2.2–2.6
Intratubular	36–38	1.5–1.6

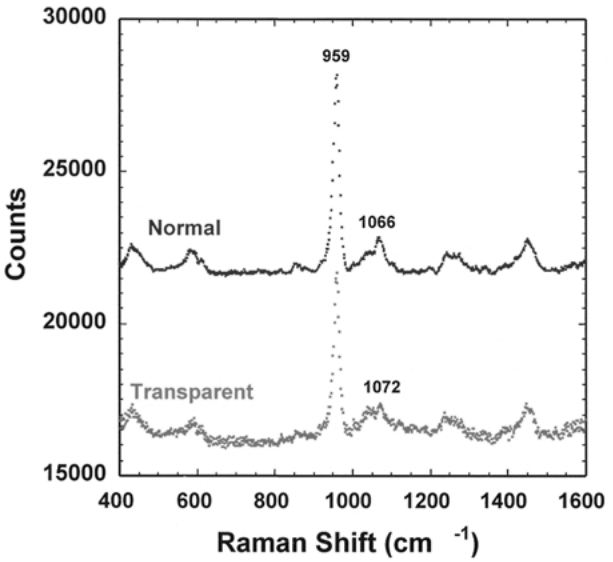

Figure 4 Raman spectroscopy of intertubular dentin showing a shift of the 1066 cm^{-1} of normal dentin to 1072 cm^{-1} in the transparent zone with decreased intensity.

sample (left side of image in Fig. 7) which revealed that the tubules exhibited less emission than the adjacent intertubular dentin. This indicates that the tubules were empty in the normal dentin as expected. In contrast,

TABLE II Raman band positions and assignments of intertubular dentin

	Normal	Transparent
$\upsilon 1PO_4^{3-}$	959	959
$\upsilon 2PO_4^{3-}$	432	432
$\upsilon 3PO_4^{3-}$	1030	1029
$\upsilon 4PO_4^{3-}$	579	580
$\upsilon 1CO_3^{2-}$	1066	1072
Amide III	1240	1240
C-H bending	1450	1450

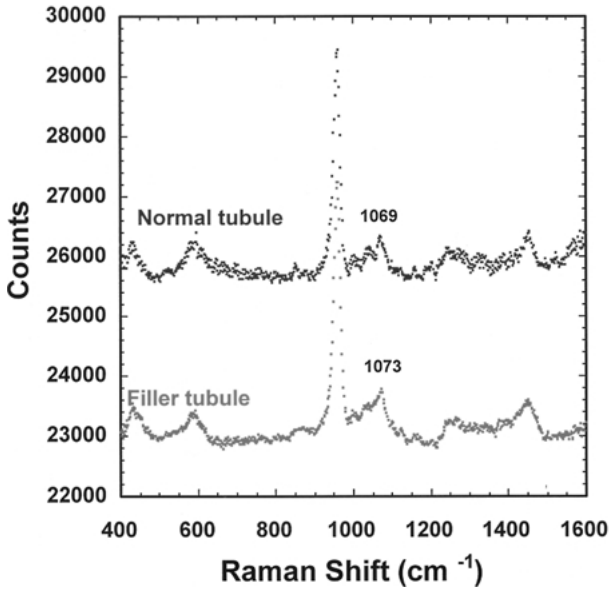

Figure 5 Raman spectroscopy of dentin tubules. The material filling the tubules (transparent zone) exhibited an increased frequency of the band near 1070 cm^{-1} as compared with the peritubular dentin in the normal dentin zone.

TABLE III Raman band positions and assignments for peritubular dentin

	Normal	Transparent
$\upsilon 1PO_4^{3-}$	960	960
$\upsilon 2PO_4^{3-}$	430	429
$\upsilon 3PO_4^{3-}$	1030	1029
$\upsilon 4PO_4^{3-}$	580	580
$\upsilon 1CO_3^{2-}$	1069	1073
Amide III	1240	1240
C-H bending	1450	1450

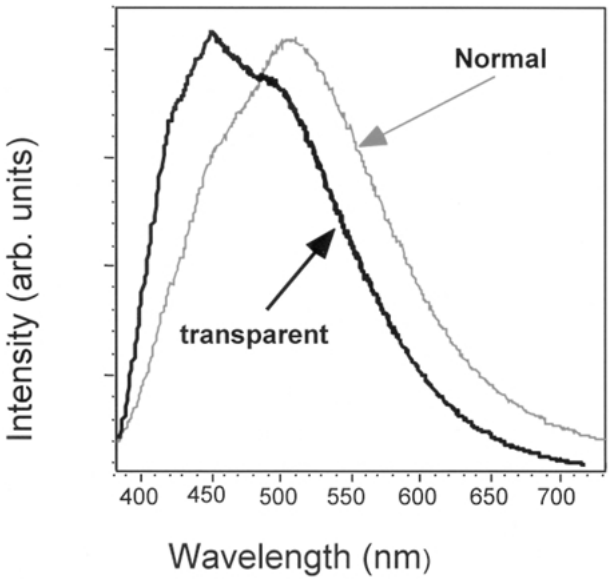

Figure 6 Emission spectra (380–730 nm) from normal and transparent dentin under 351 nm photo excitation showed a shift of the highest intensity band from 500 nm for normal dentin to 450 nm for transparent dentin. Normal dentin exhibited stronger emission in the red and near infra-red region than transparent dentin.

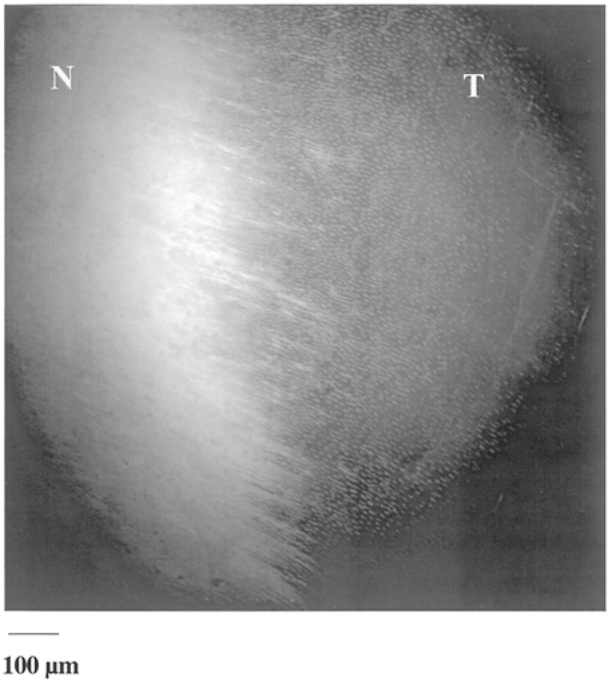

Figure 7 Emission image showing normal, transparent and the intervening transition region using a 700 nm long pass filter. Normal dentin exhibited higher intensity as compared to the transparent zone.

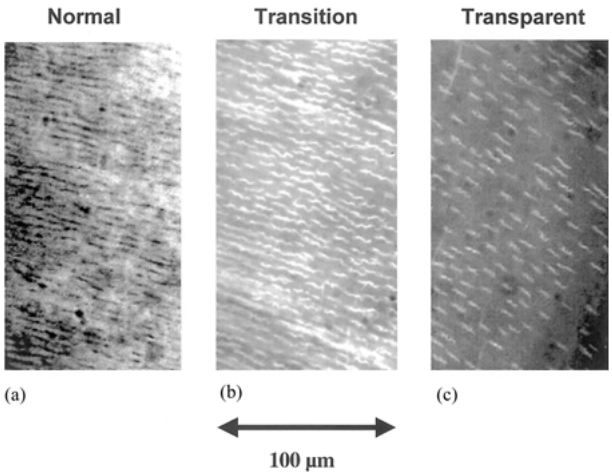

Figure 8 Higher magnification of areas shown in Fig. 7 after contrast adjustment. (a) normal zone showing less emission from tubules than the intertubular dentin since the tubules are empty; (b) transition region near the transparent zone of 250–300 μm width in which the tubules are more emissive than adjacent intertubular dentin that had emission characteristics similar to the normal dentin; (c) transparent zone.

Fig. 8(c) shows a similar image from the transparent dentin. In this region the tubules were more emissive than the intertubular dentin indicating that the tubules were filled with deposits. Fig. 8(b) shows a similar image from the same sized region in the region of transition between the other areas. The area selected was very close to the transparent region (near the center of image in Fig. 7) but was on the normal side of the transition, which is less intense.

This image indicates a transition region of 250–300 μm that lies between the normal and transparent areas in which the tubules appear to be more emissive than the adjacent intertubular dentin. The intertubular dentin in this transition region had emission characteristics similar to those seen in the normal dentin. These results suggest that in the transition zone, the tubules are filled while the intertubular dentin is apparently not altered from that of normal dentin.

Although the microscopic fluorescence image of Fig. 7 shows appreciable intensity differences between the normal and transparent regions, it is not sufficient to prove changes in chemical composition. The intensity differences could be due to different concentrations of the optically active elements in the two regions. To address this issue and to obtain better insight on the chemical characteristics of the zones, the ratio of images obtained using different spectral regions of the emission was obtained. This method takes full advantage of the different spectral characteristics of the normal and transparent dentin as shown in Fig. 6. This spectroscopic information is closely related to the chemical characteristics of the optically active material and it is independent of its concentration or the illumination intensity. Fig. 9 shows the image ratio of two 1.2 × 0.9 mm images from the section of the sample obtained using 490 to 450 nm spectral band filters. The ratio image shows that the right

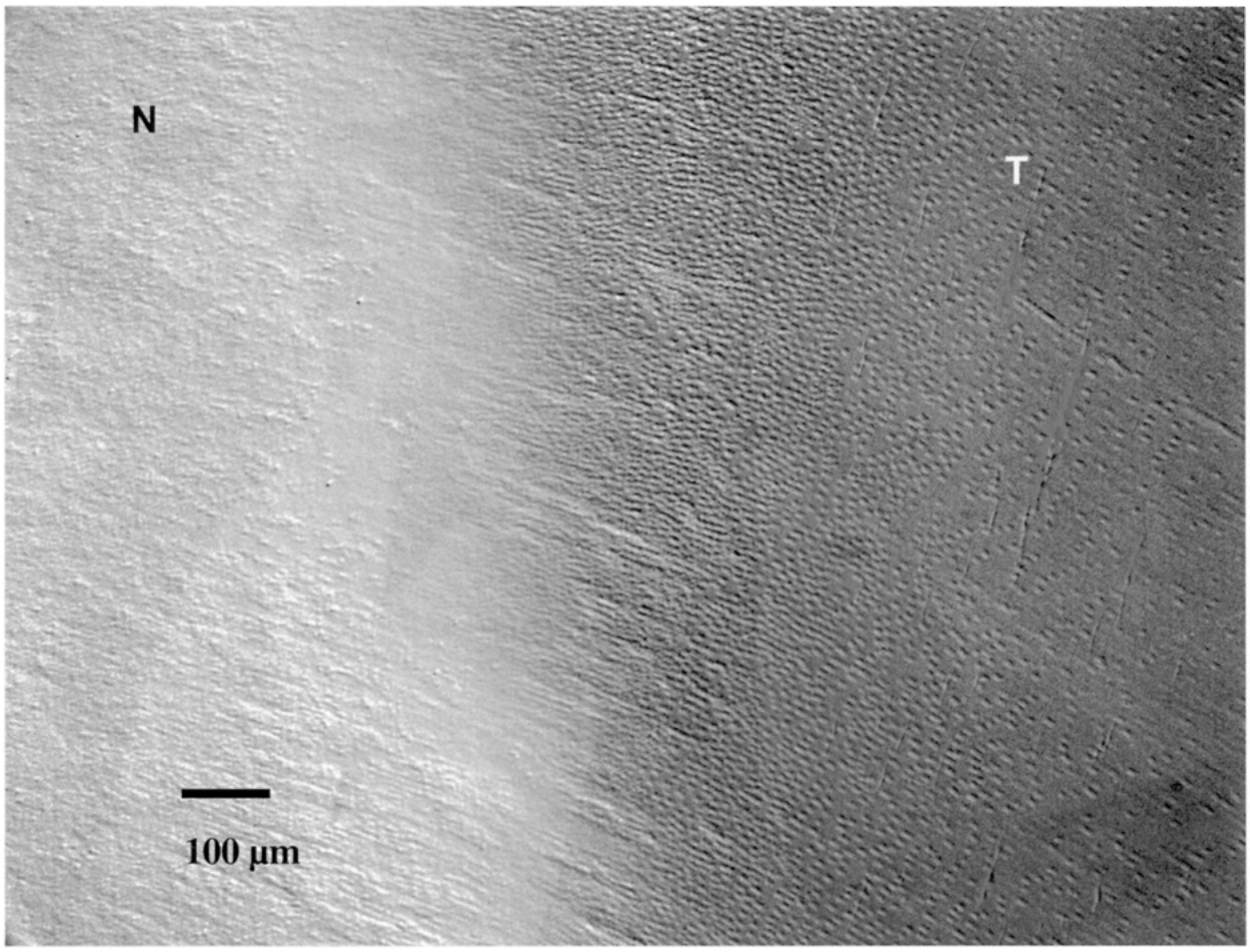

Figure 9 Ratio emission image using 490 to 450 nm spectral band filters. The transparent dentin (far right) gave much lower intensity than the normal dentin (left).

part of the image (transparent dentin) is less intense than the left part of the image from normal dentin. This is in agreement with the emission profiles shown in Fig. 6, where the ratio of the emission intensities at 490 nm over that at 450 nm is larger than 1 for normal dentin and less than 1 for the transparent dentin. The tubules, which are filled in the transparent region are clearly visible in the ratio image. The tubules were also visible in all images obtained from the ratio of any two images from image sets obtained using the five different filters that were used (three narrow-ban filters at 410, 450 and 490 nm and two long wavelength pass filters with cut-off frequencies at 450 and 700 nm). These results clearly indicate that the tubular deposits have chemical composition that differed from the transparent intertubular dentin.

As mentioned before, there is a 250–300 μm transition zone where the tubules are filled while the intertubular dentin is unaltered from that of the normal dentin. The ratio images obtained using any pair of microscopic fluorescence images show that in this transient zone very little contrast is present even though the tubules are filled. This suggests, in view of the emission spectroscopy, that the tubular deposits have emission characteristics very similar to the intertubular dentin in the transition zone, which in turn has the spectral characteristics of normal dentin. The similar emission profile of the tubular deposits and the normal dentin gives rise to the uniform contrast image in the transition zone.

4. Discussion and conclusions

Our studies of the nanomechanical properties of apparently normal and transparent dentin in the root have shown little difference in either hardness or modulus between them in either the peritubular or intertubular dentin. In addition the values seen in this study are in good agreement with values for coronal dentin [17–19]. In this work the mechanical properties of the deposits that fill the tubule lumen in the transparent zone were measured for the first time, and it was found that these properties were between the values reported for the peritubular and intertubular dentin. This suggests that the deposits may be a somewhat less dense form of mineral closely related to the peritubular dentin that forms by further precipitation of apatite on the peritubular dentin. If there are changes in the mechanical properties of the intertubular dentin, the technique was not sensitive enough to detect such small changes.

Raman spectroscopy suggests some structural or chemical differences in both intertubular dentin and the material associated with the tubule itself when comparing normal and transparent dentin. The changes in the material associated with the tubule could be a result of the additional mineral that fills or occludes the tubule, or a change in the peritubular dentin or both. We could not distinguish between these possibilities in the current work. In addition, the bands were partially obscured by a large fluorescence peak generated by laser beams of 550 and 630 nm. However, the suggestion of a chemical shift associated with the intertubular dentin in the transparent region is consistent with differences in etching characteristics seen in sclerotic lesions [7, 10, 13] and the thinner hybrid layer that has been reported for dentin bonding in such lesions [11].

In order to further demonstrate changes in chemical composition we sought to evaluate the emission characteristics of the samples. This method proved to be extremely useful and revealed significant differences between the transparent and normal dentin as well as showing a transition zone between these regions. The profound contrast between normal and transparent dentin was observed by emission spectroscopy and emission fluorescence imaging. The results suggest transparent dentin differs from normal dentin chemically, and that the material filling the tubules has emission properties close to normal dentin. This further reinforces the idea that the tubular deposits are somewhat less dense form of the apatite found in peritubular dentin, and might be formed by accretion.

Even though the luminescence intensity changes appreciably from normal to transparent dentin, it does not necessarily indicate changes in chemical composition. It has been suggested that changes in mineral concentration can affect fluorescence behavior by quenching or de-quenching as yet unidentified chromophores [20]. For example, the change in intensity could be due to the increased mineral concentration that has been observed in these zones. However, the differences in the Raman spectra between normal and transparent dentin could not be accounted for by simple increased mineralization. In particular, the shift in the carbonate peak at $1066\,cm^{-1}$ is suggestive of an altered metallic ion substitution for Ca in the transparent zone. These results strongly suggest that the intertubular dentin of the transparent region in non-carious cervical lesions, that are also frequently termed sclerotic, are chemically altered from that of normal root dentin. Thus the formation of such transparent dentin is associated with formation of mineral deposits within the tubule lumen that are probably apatite like, while the intertubular dentin is chemically modified as well. The exact nature of the chemical changes induced in the intertubular dentin of the transparent region require further study, but these changes appear to lead to little change in the mechanical properties of the intertubular dentin. However, these changes do appear to have a significant effect on bonding characteristics as indicated by formation of thinner hybrid layer during dentin bonding [11].

References

1. L. C. LEVITCH, J. D. BADER, D. A. SHUGARS and H. O. HEYMAN, *J. Dent.* **22** (1994) 195.
2. D. F. WEBER, *Archs. Oral. Biol.* **19** (1974) 163.
3. M. BRÄNNSTRÖM and R. GARBEROGLIO, *Swed. Dent. J.* **4** (1980) 87.
4. L. VASILIADIS, A. I. DARLING and B. G. H. LEVERS, *Archs. Oral. Biol.* **28** (1983) 693.
5. M. YOSHIYAMA, J. MASADA, A. UCHIDA and H. ISHIDA, *J. Dent. Res.* **68** (1989) 1498.
6. T. YAGI and S. SUGA, *Shigaku* **78** (1990) 313.
7. E. S. DUKE and J. LINDEMUTH, *Am. J. Dent.* **3** (1990) 264.
8. E. S. DUKE, J. W. ROBINS and D. S. SNYDER, *Quintessence Int.* **22** (1991) 889.
9. H. O. HEYMAN and S. C. BAYNE, *J. Am. Dent. Assoc.* **124** (1993) 27.

10. J. A. GWINNETT and M. D. JENDRESEN, *J. Dent. Res.* **57** (1978) 543.
11. B. VAN MEERBEEK, M. BRAEM, P. LAMBRECHTS and G. VAHERLE, *J. Dent.* **22** (1994) 141.
12. J. PERDIGAO, E. J. SWIFT, G. E. DENEHY, J. S. WEFEL and K. J. DONLY, *J. Dent. Res.* **73** (1994) 44.
13. G. W. MARSHALL, Y. J. CHANG, K. SAEKI, S. A. GANSKY and S. J. MARSHALL, *J. Biomed. Mater. Res.* **49** (2000) 338.
14. J. M. WHITE, H. E. GOODIS, S. J. MARSHALL and G. W. MARSHALL, *J. Dent. Res.* **73** (1994) 1560.
15. M. BALOOCH, I. C. WU-MAGIDI, A. S. LUNDKVIST BALAZS, S. J. MARSHALL, G. W. MARSHALL, W. J. SEIKHAUS and J. H. KINNEY, *J. Biomed. Mater. Res.* **40** (1998) 539.
16. M. F. DOERNER and W. D. NIX, *J. Mater. Res.* **1** (1986) 601.
17. J. H. KINNEY, M. BALOOCH, S. J. MARSHALL, G. W. MARSHALL and T. P. WEIHS, *J. Biomech. Eng.* **118** (1996) 133.
18. *Idem.* S.J. MARSHALL, G. W. MARSHALL, T. P. WEIHS *Arch. Oral. Biol.* **41** (1996) 9.
19. J. H. KINNEY, M. BALOOCH, G. W. MARSHALL and S. J. MARSHALL, *ibid.* **44** (1999) 813.
20. M.H. VAN DER VEEN and J.J. BOSCH *Caries Res.* **30** (1996) 93.

Received 15 December 1999
and accepted 26 January 2000